Journal of Power Sources 215 (2012) 288–295

Contents lists available at SciVerse ScienceDirect

Journal of Power Sources

journal homepage: www.elsevier.com/locate/jpowsour

The effects of temperature on the electrochemical performance of sodium–nickel chloride batteries

Xiaochuan Lu, Guosheng Li, Jin Y. Kim*, John P. Lemmon, Vincent L. Sprenkle, Zhenguo Yang

Pacific Northwest National Laboratory, Energy Materials, 902 Battelle Blvd., P.O. Box 999, Richland, WA 99352, USA

HIGHLIGHTS

- A planar-type sodium–nickel chloride battery with a thin BASE was tested at low temperatures.
- The battery was able to be cycled at C/3 rate at as low as 175 °C.
- Low operating temperature resulted in an improvement in the stability of cell performance.
- Performance degradation at higher temperatures was related to the particle growth in the cathode.

ARTICLE INFO

Article history:
Received 20 March 2012
Received in revised form
9 May 2012
Accepted 10 May 2012
Available online 18 May 2012

Keywords:
Sodium–nickel chloride battery
β″-Al_2O_3 solid electrolyte (BASE)
Low temperature
Planar design

ABSTRACT

Sodium–nickel chloride (ZEBRA) batteries are typically operated at relatively high temperatures (^{3} 300 °C) to achieve adequate electrochemical performance. In the present study, the effects of operating temperature on the electrochemical performance of planar-type Na/$NiCl_2$ batteries were investigated to evaluate the feasibility of battery operation at low temperatures (£200 °C). The planar-type cell was able to be cycled at C/3 rate at as low as 175 °C despite higher cell polarization. Overall, low operating temperature resulted in a considerable improvement in the stability of cell performance. Cell degradation was negligible at 175 °C, while 55% increase in end-of-charge polarization was observed at 280 °C after 60 cycles. SEM analysis indicated that the degradation at higher temperatures was related to the particle growth of both nickel and sodium chloride. The cells tested at lower temperatures (£200 °C), however, exhibited a sharp drop in voltage at the end of discharge due to the diffusion limitation, possibly caused by the limited ionic conductivity of catholyte or the poor wettability of sodium on the β″-Al_2O_3 solid electrolyte (BASE). Therefore, improvements in the ionic conductivity of catholyte and sodium wetting as well as reduction in the ohmic resistance of BASE are required to enhance the battery performance at low temperatures.

Published by Elsevier B.V.

1. Introduction

Sodium–beta alumina batteries (NBBs), based on the molten Na anode and the β″-Al_2O_3 solid electrolyte (BASE), have received increasing attention over the past few decades as an energy storage device for renewable energy and electric vehicles [1–3]. The NBBs reversibly store and release electrical energy via sodium ion transport across the BASE between positive and negative electrodes.

Two types of NBBs depending on cathode materials have been widely investigated. The first one is the sodium–sulfur (Na–S) battery of which cathode is molten sulfur, following the cell reaction:

$$xS + 2Na \rightarrow Na_2S_x \quad (x = 5 \sim 3), \quad E = 2.08 \sim 1.78 \text{ V at } 350\,^{\circ}C \tag{1}$$

The Na–S chemistry offers a few attractive features such as high theoretical energy density (~760 Wh kg^{-1}), high energy efficiency and good cycle life. The other type of NBBs is the so-called ZEBRA battery in which solid transition metal halides such as $NiCl_2$ and $FeCl_2$ are used as active cathode materials [4–7]. The ZEBRA battery needs a molten secondary electrolyte such as $NaAlCl_4$ (melting point = 157 °C) in the cathode so as to ensure facile sodium ion transport between the BASE and solid cathode materials. The electrochemical reaction of Na–$NiCl_2$ cells is as follows:

$$NiCl_2 + 2Na \rightarrow Ni + 2NaCl \quad E = 2.58 \text{ V at } 300\,^{\circ}C \tag{2}$$

The ZEBRA battery exhibits a number of advantages over the Na–S battery, which include higher voltage, easiness of

* Corresponding author. Tel.: +1 509 375 2225; fax: +1 509 375 2186.
E-mail address: Jin.Kim@pnnl.gov (J.Y. Kim).

0378-7753/$ – see front matter Published by Elsevier B.V.
doi:10.1016/j.jpowsour.2012.05.020

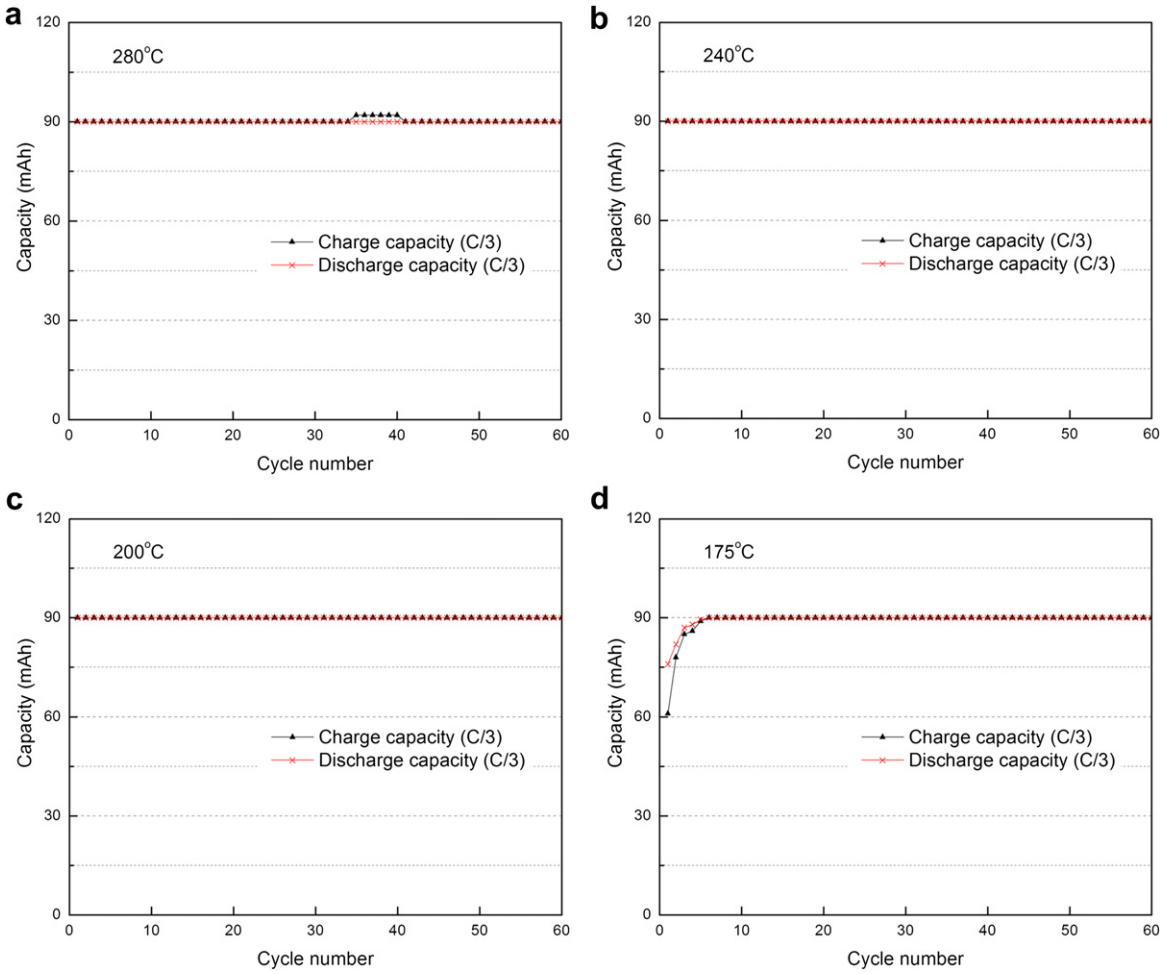

Fig. 1. Charge and discharge capacity of the cells tested at (a) 280 °C, (b) 240 °C, (c) 200 °C and (d) 175 °C.

assembly in discharged state, less corrosive nature of cathode materials, safer cell failure mode, and better tolerance against overcharging [3].

Several technical issues have been addressed in terms of optimizing the performance of the ZEBRA battery: the formation of low-conducting nickel chloride [8,9], the solubility of nickel chloride in $NaAlCl_4$ melt [10] and cell capacity fade with time [5]. These problems have been by and large mitigated by using additives such as sodium bromide, sodium iodide, sulfur, aluminum, iron, and iron sulfide [5,8,9]. The ZEBRA battery is usually operated at relatively high temperatures over 300 °C in order to achieve adequate battery performance by reducing the ohmic resistance of thick BASE (1–3 mm thick) used in typical tubular cells and improving the ionic conductivity of secondary electrolyte [3,11]. The Zebra battery is known to experience the performance degradation due to particle ripening and side reactions occurring in the cathode [12,13]. Since these degradation mechanisms are expected to be enhanced at high operating temperatures, lowering the temperature (≤200 °C) may lead to improved cycle life. The reduced temperature technology may also enable to use low cost materials of sealing and construction and to incorporate high throughput manufacturing methods, providing a path towards broad market penetration for grid storage. However, no research has been reported up to now regarding low-temperature performance of the Zebra battery.

In the present work, the effects of temperature on the electrochemical performance and the microstructural change of $Na/NiCl_2$ Zebra batteries were investigated to figure out feasibility and possible technical issues related to low-temperature operation.

2. Experimental

2.1. Fabrication of BASE discs

BASE discs were fabricated using the vapor phase process [3,13–16]. Starting powders were high purity α-Al_2O_3 (Almatis, >99.8%) and yttria-stabilized zirconia (UCM Advanced Ceramics, 8 wt% yttria-stabilized zirconia). 70 vol% α-Al_2O_3 and 30 vol% YSZ were ball milled with a dispersant (Phospholan PS-236, Akzo Nobel), solvents (MEK/Ethanol), a plasticizer (benzyl butyl phthalate, Aldrich) and a binder (Butvar® B-79) to make slurry. After the slurry was cast into a thin sheet (~125 μm), the sheets were laminated and laser-cut to form circular discs. The discs were fired at 1600 °C in air to achieve full density (>99%). The sintered α-Al_2O_3/YSZ discs were then placed in loose β″-Al_2O_3 powder and heat-treated at 1450 °C in air in order to convert α-Al_2O_3 into β″-Al_2O_3. The β″-Al_2O_3 powder used in the conversion process was synthesized using boehmite, Na_2CO_3 and Li_2CO_3 via a solid-state reaction [3,17]. The conversion occurred by a coupled transport of sodium and oxygen ions from the β″-Al_2O_3 powder to the samples [18]. The thickness of the converted composite β″-Al_2O_3/YSZ discs was ~600 μm.

2.2. Cell construction and testing

The schematic of a single cell was shown in our previous publications [13,16]. A BASE disc with the diameter of 26 mm was glass-sealed to an α-Al_2O_3 ring (active cell area: ~3 cm^2). The cell was assembled in a glove box with 1 g of cathode granules consisting of Ni, NaCl and small amounts of additives. After the granules were dried at 270 °C under vacuum to remove all traces of moisture, molten $NaAlCl_4$ secondary electrolyte was infiltrated into the cathode. A foil and a spring made of Mo were placed on the top of the cathode as a current collector. A spring-loaded stainless steel shim, which served as a molten sodium reservoir, was inserted into the anode compartment. Anode and cathode end plates were then compression-sealed to both sides of α-Al_2O_3 ring using gold o-rings. Nickel leads, which served as current collectors, were welded to the electrode end plates.

The assembled cell was heated in air to 280 °C at which it was initially charged up to 2.8 V under the constant current of 10 mA. The cell was then discharged back to 80% of the initial maiden charge capacity using the same current. After the initial cycle, the cell was cooled down to various temperatures between 175 °C and 280 °C and cycled between 20 and 80% of the maiden charge capacity. The cycling was conducted under the constant current of 30 mA, which corresponded to C/3 rate for the cycling capacity of 90 mAh. The voltage limits of 2.8 and 1.8 V were applied to avoid overcharging and overdischarging, respectively. Cell testing was carried out using an electrochemical interface (Solartron 1287, Solartron Analytical). The electrochemical impedance spectra were obtained under open-circuit voltage (OCV) after charge and discharge using the electrochemical interface and a frequency response analyzer (Solartron 1260, Solartron Analytical). The frequency range was 2 MHz to 0.01 Hz, and the ac amplitude was 10 mV. The microstructure of the cathode was also analyzed using a scanning electron microscope (SEM, JEOL JSM-5900LV) after a cell finished the discharge step of the 60th cycle.

3. Results and discussion

Fig. 1 shows the charge and discharge capacities of cells cycled at various temperatures under C/3 rate. In the temperature range between 280 °C and 200 °C, cells were cycled with the full capacity of 90 mAh (refer to Fig. 1a–c). When a cell was cycled at the lower temperature of 175 °C, it revealed the lower capacity of 60 and 75 mAh for the first charge and discharge, respectively (see Fig. 1d). Asymmetric cycling was observed up to the 5th cycle suggesting the cell had been cycled further in the discharged state after each cycle until the full capacity was achieved. However, the reversible cycling capacity increased with continued cycling and reached the full capacity of 90 mAh after five cycles. Reasons for this abnormal behavior will be discussed in detail later. As previously mentioned, the sodium-nickel chloride battery typically operates at 300 °C or above due to the high ohmic resistance of a thick BASE and the limited ionic conductivity of molten $NaAlCl_4$. However, these results clearly show that a cell exhibits reasonable electrochemical performance (~60% of theoretical capacity at C/3 rate) at reduced temperatures as low as 175 °C.

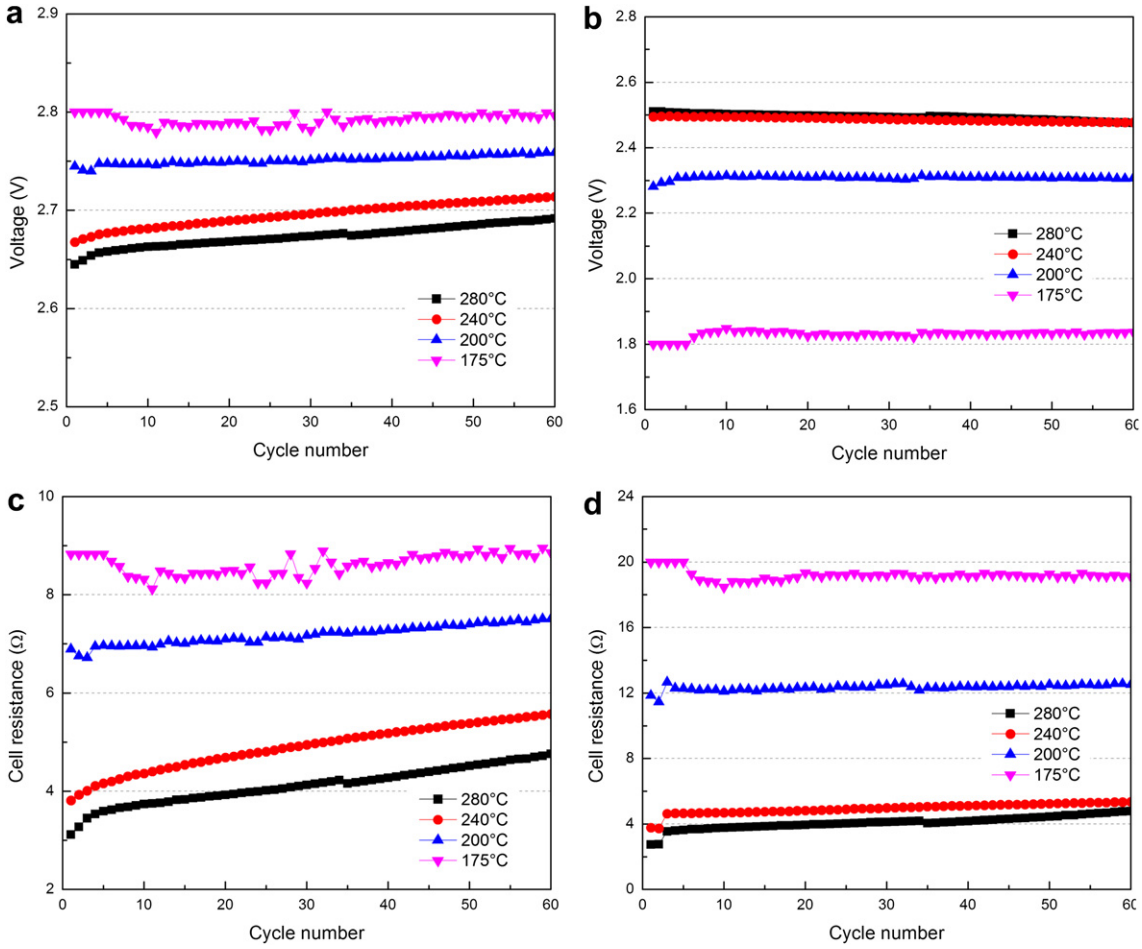

Fig. 2. Cell voltage and corresponding cell polarization of the cells tested at various temperatures: (a) end-of-charge voltage, (b) end-of-discharge voltage, (c) cell polarization at the end of charge and (d) cell polarization at the end of discharge.

The cell voltage at the end of each cycling step (charge and discharge) and the corresponding cell polarization are shown in Fig. 2. As expected, the overpotential depends on temperature with the lowest cell temperature exhibiting the highest cell overpotential (see Fig. 2c and d). Factors contributing to the increased overpotential include: the higher ohmic resistance of BASE, the reduced ionic conductivity of $NaAlCl_4$, decreased electrochemical reaction kinetics, and insufficient sodium wetting on the anode side of the BASE. The higher polarization at the lower temperature yields the larger overpotential for both charging and discharging, leading to a higher cell voltage for charge and a lower voltage for discharge (refer to Fig. 2a and b). As shown in Fig. 1, no capacity fade was observed for all cells during 60 cycles, meaning that both charge and discharge were not interrupted by the voltage limits except an initial few cycles of the cell tested at 175 °C. However, the increase in cell polarization as well as the change in end voltages indicates that the degradation of cell performance occurred during cycling, especially at higher temperatures. The end-of charge polarization increased 55% and 47% after 60 cycles at 280 °C and 240 °C, respectively. On the other hand, the increase in cell polarization at lower temperatures was much lower (9% increase at 200 °C and almost negligible at 175 °C). A similar trend was detected from the cell polarization at the end of discharge. These results clearly imply that the operating temperature is one of key factors which influence the stability of cell performance.

Fig. 3 shows the plots of voltage as a function of the state of charge (SOC) for 1st, 3rd, 6th and 20th cycles at various temperatures. Overall, the voltage at the start of charge and discharge is quite stable throughout the cycling while the voltage at end of charge and discharge changes significantly especially at the high temperature of 280 °C. Since the amounts of reactants for the electrochemical reactions decreases during each step (charge or discharge), the degradation in cell performance (indicated by the increase in cell polarization at the end of each step) can be observed more obviously at the end of each step. At the temperature of 200 °C or above (refer to Fig. 3a and b), the cells were successfully cycled between 20% and 80% of the maiden charge capacity even though some cell degradation was observed. At 175 °C, the 1st charge started at 20% SOC, and only ~40% (~60 mAh) of the maiden charge capacity was charged due to high cell polarization before the charge was stopped by reaching the charge voltage cut off limit of 2.8 V. The 1st discharge proceeded down to 10.2% SOC until it stopped at the low voltage limit of 1.8 V, resulting in the more discharge capacity (75 mAh) than the charge capacity (60 mAh). This phenomenon continued until the cycling of the cell became stable after 5th cycle. Thus, the cycling window gradually shifted to the more discharged state until the full capacity of 90 mAh were charged and discharged in the range of 6%–66% SOC (see Fig. 3(c)). The initial abnormal behavior observed in Fig. 1(d) is the result of limited charging capability within the given voltage window. One notable behavior of the cells tested at lower temperatures (e.g. 175 and 200 °C) was a precipitous voltage decrease at the end of discharge. This phenomenon is related to the diffusion limitation which is possibly caused by the high viscosity and the low ionic conductivity of $NaAlCl_4$ at low operating temperatures close to its melting point. The high viscosity and the corresponding low Na^+ conductivity can cause the diffusion limitation at the end of discharge at which the reaction zone moves far

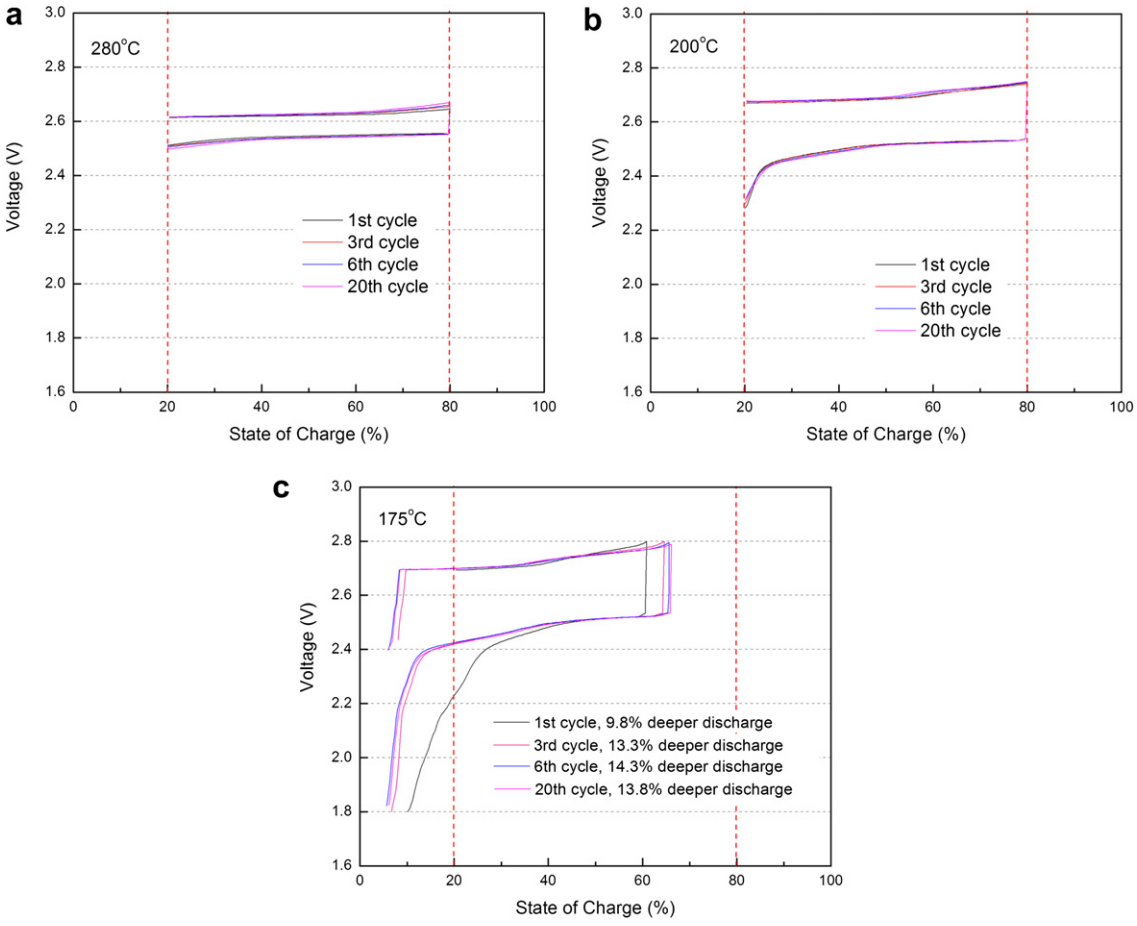

Fig. 3. Charge and discharge curves (voltage vs. state of charge) of the cells tested at (a) 280 °C, (b) 200 °C and (c) 175 °C.

from the cathode/BASE interface. Another possible cause is poor sodium wetting to the BASE at low temperatures. At the end of discharge, only 20% of the molten sodium is left on the anode side. While 20% of sodium is enough to transport sodium from the anode to the BASE at 280 °C where sodium wetting is good, it may not be sufficient enough to ensure the good coverage of molten sodium on the BASE due to poor wettability at the temperature of 200 °C or below. The combined effects of the poor sodium wettability and the significantly decreased amount of sodium at the end of discharge at 175 °C (only ~6% sodium left) possibly caused a sharper drop in voltage compared to 200 °C. Narrowing the cycling SOC window may help to avoid a significant drop in voltage during discharge and to minimize energy efficiency loss at the lower temperatures.

The impedance spectra of the cells tested at various temperatures are shown in Fig. 4. The data were obtained under OCV after the end of charge and discharge of 30th and 60th cycles. The impedance spectra exhibited depressed semicircles with a peak frequency less than 100 Hz and a line at lower frequencies, which was typically related to mass transport diffusion processes. Overall, the ohmic resistance was slightly higher after the end of charge compared to the end of discharge. This is related to the formation of low-conducting $NiCl_2$ on Ni particles [8,9]. The ohmic resistance (R_{ohmic}) obtained from the impedance spectra and the total cell polarization (R_{total}) measured by the DC method is listed in Table 1. At the high temperature of 240 °C or above, both the total cell polarization and the ohmic resistance increased with cycles from 30th to 60th cycle, while they are pretty stable at the low temperature of 200 °C or below. Table 2 lists area-specific resistance (ASR) of our composite BASE (R_{BASE}) and cell ohmic resistance compared with BASE used in conventional state-of-the-art tubular sodium batteries. The ASR of our composite BASE [19] was quite consistent with that of composite tubular BASE reported by SICCAS [20], even though it was higher than that of pure BASE [21]. It should be also noted that the contribution of BASE towards the ohmic resistance of Na–$NiCl_2$ cells tested in this study was more than 90%. Therefore, decrease in the ohmic resistance of BASE is the one of the technical issues to improve the cell performance further at low temperatures.

Table 1
Ohmic resistance and total cell polarization of the cells after 30 and 60 cycles.

	After 30th cycle				After 60th cycle			
	End of charge		End of discharge		End of charge		End of discharge	
	R_{ohmic}	R_{total}	R_{ohmic}	R_{total}	R_{ohmic}	R_{total}	R_{ohmic}	R_{total}
280 °C	0.72	0.97	0.72	1.23	0.77	1.05	0.76	1.31
240 °C	0.93	1.41	0.88	1.57	0.96	1.53	0.91	1.63
200 °C	1.43	2.23	1.41	2.60	1.46	2.28	1.43	2.64
175 °C	1.52	2.81	1.49	2.79	1.52	2.82	1.52	2.80

Unit: Ω.

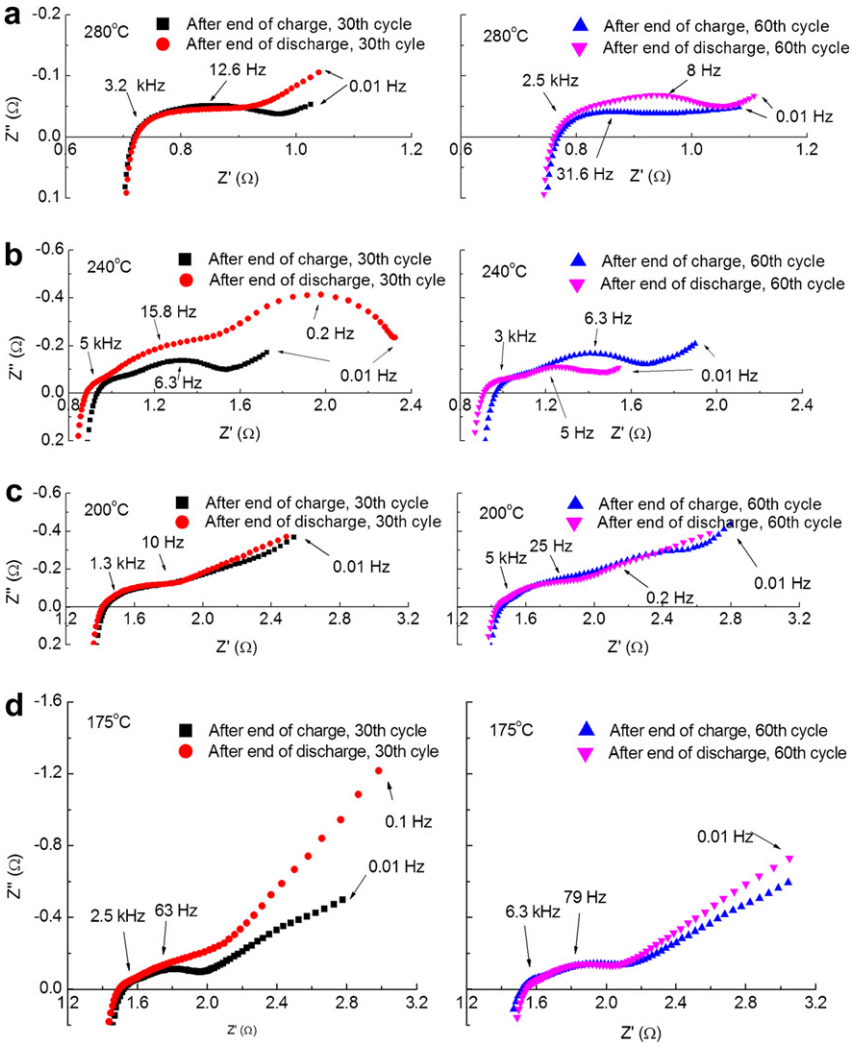

Fig. 4. Impedance spectra of the cells tested at (a) 280 °C, (b) 240, (c) 200 °C and (d) 175 °C.

Table 2
Area specific resistance (ASR) of BASE and cell ohmic resistance compared with that of conventional state-of-the-art tubular sodium battery.

	This study		SICCAS [20]		Ionotec [21]
	R_{BASE} (β''-Al_2O_3 + ~30 vol% ZrO_2) [19]	R_{ohmic}	R_{BASE} (pure β''-Al_2O_3)	R_{BASE} (β''-Al_2O_3 + 20 vol% ZrO_2)	R_{BASE} (pure β''-Al_2O_3)
300 °C	1.65	–	0.86[a]	1.65[a]	0.63[a]
280 °C	2.0	2.16	–	–	–
240 °C	2.69	2.79	–	–	–
200 °C	3.91	4.29	–	–	1.5[a]

Unit: Ω cm^2.
[a] Assuming the thickness of BASE tube is 1.5 mm.

In the current study, it was found that a higher operating temperature caused a more degradation. To identify the degradation mechanisms, the microstructure of the cathode was observed after the discharge of 60th cycle using SEM. Fig. 5 shows the elemental mapping of Ni and Na as well as SEM micrographs obtained from the fracture surface of the cells tested at various temperatures. Even though Ni was detected in the entire cathode layer regardless of operating temperatures, the difference in particle size was observed. The selected magnified backscattered images of the corresponding samples (refer to Fig. 6) clearly show the enhanced growth of Ni particles (white particles) at high temperatures. For the cell tested at 175 °C (Fig. 6e), the size of nickel

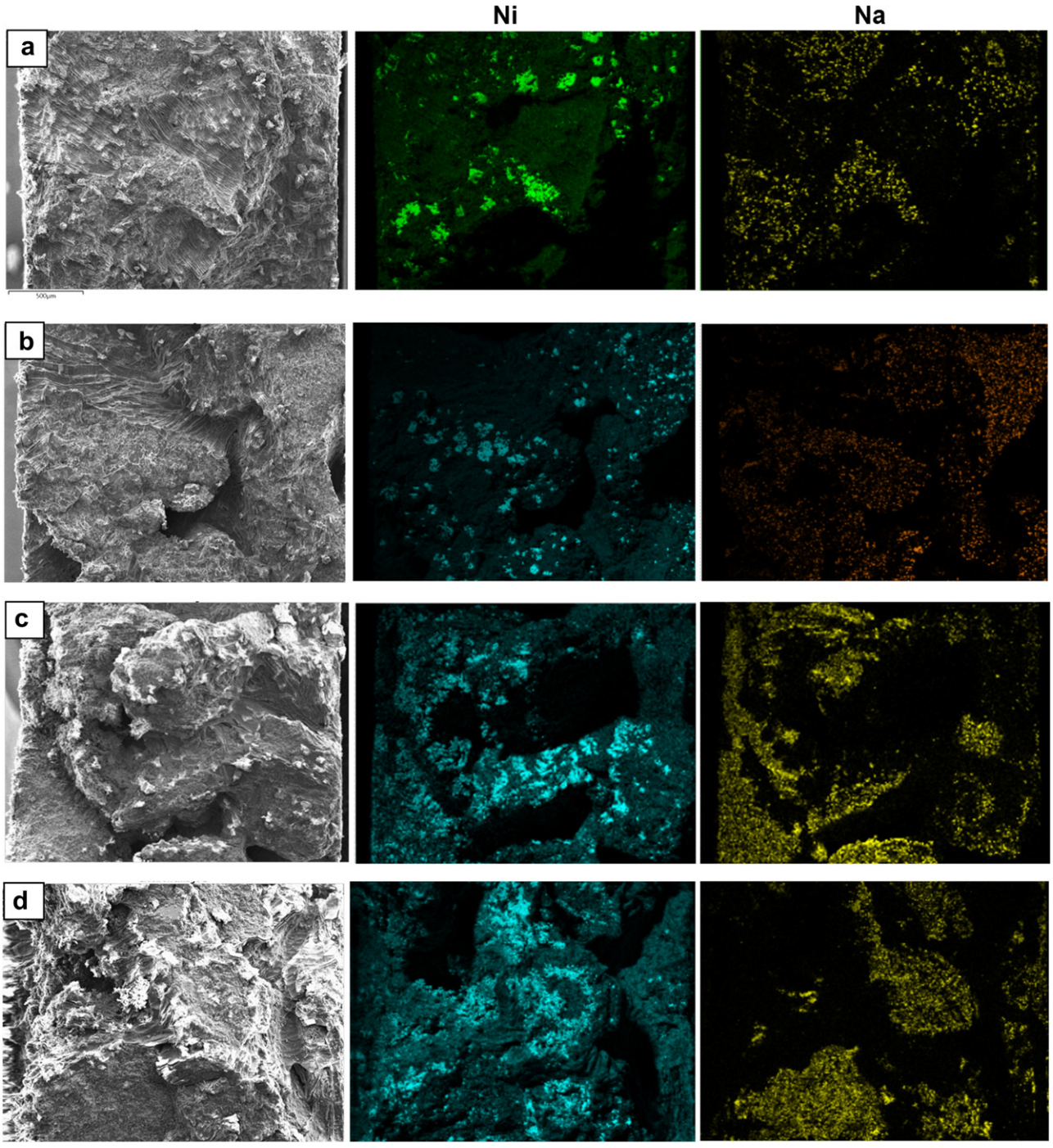

Fig. 5. SEM micrographs and elemental mapping of Ni and Na collected from the fracture surfaces of the cathodes after operating at (a) 280 °C, (b) 240, (c) 200 °C and (d) 175 °C.

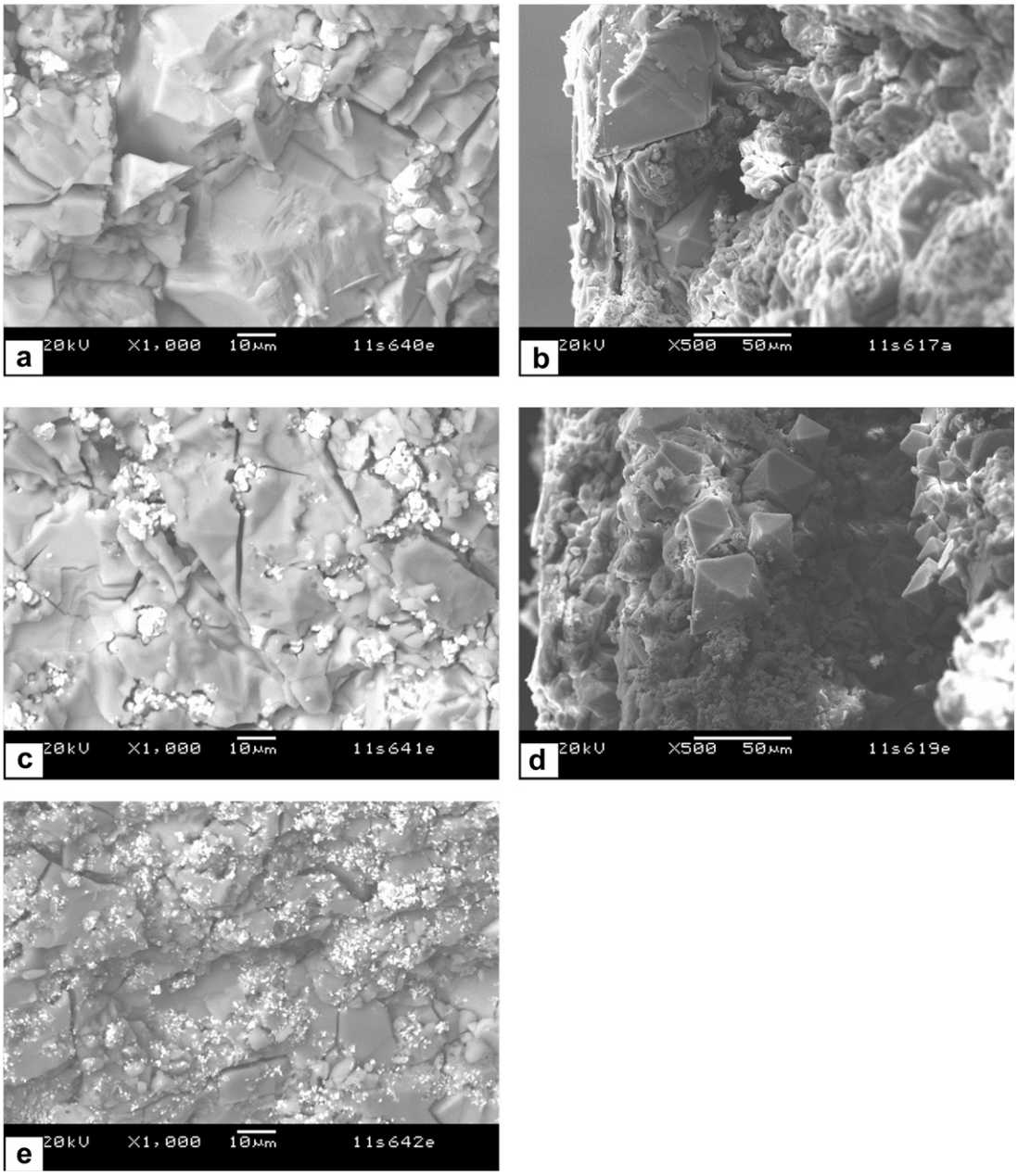

Fig. 6. Backscattered electron images of the cathodes after operating at: (a and b) 280 °C, (c and d) 240 °C and (e) 175 °C.

particles (bright particles) is ≤1 μm, which is similar to the original size of the raw nickel powder. However, the Ni particle size of the cells operated at 240 °C and 280 °C are 3–5 μm and 7–10 μm, respectively. These results clearly indicate that cycling at high operating temperatures facilitates the coarsening of nickel particles and hence the decrease in surface area of Ni. Therefore, the more rapid degradation in cell performance at higher temperature can be attributed to the enhanced coarsening of Ni particles, which causes the significant reduction in electrochemically active sites. Since only approximately one-third of nickel was involved in the electrochemical reaction and the rest worked as an electrical conduction pathway, the growth of nickel particles can also induce the increase in ohmic resistance by deteriorating electrical contact between nickel particles. Thus, the increase in ohmic resistance with cycling observed at high temperatures (refer to Table 1) is likely owing to the nickel coarsening.

The sodium chloride particle growth can be another factor responsible for cell degradation [13]. Small sodium chloride particles were consumed during charge and redistributed on the surface of large particles during the subsequent discharge. As such, the large sodium particles became larger while the small ones disappeared with cycling. The crystal growth of NaCl can apparently cause similar effects as nickel coarsening in terms of degradation in cell performance due to the decrease in reaction sites and hence causing the higher cathode polarization. Fig. 6(b) shows large NaCl crystals (~50 μm in size) in cells tested at 280 °C. When the operating temperature was lower, the smaller NaCl crystals were observed. The size of NaCl crystals in the cell tested at 240 °C was ~30 μm (Fig. 6d) while no large NaCl crystals were observed in the cell operated at 175 °C (Fig. 6e). The higher particle growth rate of both nickel and sodium chloride observed in the cell operated at high temperatures is likely responsible for the degradation in cell performance.

4. Conclusion

A sodium–nickel chloride battery with a planar composite BASE was successfully cycled under C/3 rate at reduced temperatures as low as 175 °C, even though the operation at lower temperatures in general caused higher cell polarization. One notable behavior of the cells tested at lower temperatures (175 and 200 °C) was a sharp drop in voltage at the end of discharge. This phenomenon was related to the diffusion limitation possibly caused by the low ionic conductivity of $NaAlCl_4$ melt or the poor wettability of sodium on the BASE at reduced temperatures. Operating temperature gave significant influences on the stability of cell performance during cycling. Overall, the higher operating temperature resulted in the more rapid increase in cell polarization with cycling. 55% increase in end-of-charge polarization was observed at 280 °C after 60 cycles, while little change was found in the cell tested at 175 °C. SEM analysis indicated that the performance degradation at higher temperatures was due to the particle growth of both nickel and sodium chloride in the cathode. These results indicate that the cell operation below 200 °C is feasible and also provides better stability. To improve the performance at low operating temperatures further, more efforts need to be made in terms of improving the ionic conductivity of BASE and catholyte as well as overcoming the wetting problem of liquid sodium.

Acknowledgements

The work is supported by Laboratory-Directed Research and Development Program (LDRD) of the Pacific Northwest National Laboratory (PNNL) and the Office of Electricity Delivery & Energy Reliability's storage program. PNNL is a multiprogram laboratory operated by Battelle Memorial Institute for the Department of Energy under Contract DE-AC05-76RL01830.

References

[1] J.T. Kummer, in: H. Reiss, J.O. McCaldin (Eds.), Beta-Alumina Electrolytes, Pergamon Press, New York, 1972, pp. 141–175.
[2] J.L. Sudworth, A.R. Tilley, The Sodium Sulphur Battery, Chapman & Hall, London, 1985.
[3] X. Lu, G. Xia, J.P. Lemmon, Z. Yang, J. Power Sources 195 (2010) 2431.
[4] R.C. Galloway, J. Electrochem. Soc. 134 (1987) 256.
[5] R.J. Bones, D.A. Teagle, S.D. Brooker, F.L. Cullen, J. Electrochem. Soc. 136 (1989) 1274.
[6] R.J. Bones, J. Coetzer, R.C. Galloway, D.A. Teagle, J. Electrochem. Soc. 134 (1987) 2379.
[7] P.T. Moseley, R.J. Bones, D.A. Teagle, B.A. Bellamy, R.W.M. Hawes, J. Electrochem. Soc. 136 (1989) 1361.
[8] L. Redey, D.R. Vissers, J. Prakash, U.S. Pat. 5,283,135 (1994) U.S. Pat. 5,340,668(1994).
[9] J. Prakash, L. Redey, D.R. Vissers, J. Electrochem. Soc. 147 (2000) 502.
[10] L. Redey, C. Rose, R. Lowrey, Ext. Abstr., Electrochem. Soc. Meeting (1992).
[11] J.L. Sudworth, J. Power Sources 100 (2001) 149.
[12] Tannaz Javadi, Anthony Petric, J. Electrochem. Soc. 158 (2011) A700.
[13] X. Lu, G.W. Coffey, K.D. Meinhardt, V.L. Sprenkle, Z. Yang, J.P. Lemmon, ECS Trans. 28 (2010) 7.
[14] A.V. Virkar, J.-F. Jue, K.-Z. Fung, U.S. Pat. 6,117,807 (2000).
[15] P. Parthasarathy, N. Weber, A.V. Virkar, ECS Trans. 6 (2007) 67.
[16] X. Lu, J.P. Lemmon, V.L. Sprenkle, Z. Yang, JOM. J. Minerals, Metals Mater. Soc. 62 (2010) 31.
[17] A. Vanzyl, M.M. Thackeray, G.K. Duncan, A.I. Kingon, R.O. Heckroodt, Mater. Res. Bull. 28 (1993) 145.
[18] A.V. Virkar, A High Temperature Electrochemical Energy Storage System Based on Sodium Beta″-Alumina Solid Electrolyte (BASE), Report to DOE (2008).
[19] http://www.sandia.gov/ess/docs/pr_conferences/2011/3-SPRENKLE_2011_OE_Na_Battery_Review_final.pdf.
[20] Z. Wen, Z. Gu, X. Xu, J. Cao, F. Zhang, Z. Lin, J. Power Sources 184 (2008) 641.
[21] http://www.ionotec.com/pdfs/NaKbetaceramics.pdf.